JOURNAL OF MATERIALS SCIENCE 30 (1995) 6288–6298

On the thin-section size dependent creep strength of a single crystal nickel-base superalloy

A. BALDAN
Department of Mechanical Engineering, Eastern Mediterranean University, G. Magosa, Mersin 10, Turkey

The combined effects of thin-section size, D, and microcracks on the creep behaviour of the single crystal MAR-M 0 0 2 were investigated at the creep conditions of 300 MPa and 900 °C. It was observed that the creep rupture life, t_R is controlled by the mean microcrack size to thin-section size, (d_c/D), (or the total number, (N_m), of the mean-sized microcrack particles across the diameter, assuming $D/d_c = N_m$); reducing N_m continuously improves t_R. The creep rupture strain (or ductility), ε_R, can be improved sharply by increasing the total number, N_T, of microcrack particles across the cross-section, $N_T \propto D^2 N_A$, where N_A is the number of microcrack particles (cavity density) per cross-section. The behaviour of the creep rupture ductility was interpreted in terms of the weakest link, or "largest-flaw" concept; the observation of the higher proportion of the less likely dangerous (smaller in size) microcracks with increasing N_T was the underlining reason for the improvement in ductility.

1. Introduction

The use of single crystal (SC) nickel-base superalloys for aeroengine turbine blades and other high temperature items has enabled significantly increased turbine inlet temperatures. The SC superalloys, without grain boundary strengthening elements, developed in the late 1970s along with high temperature solution heat treatments, greatly improved resistance to high temperature creep, thermal fatigue and low and high cycle fatigue [1, 2]. Since then, nickel-base SC superalloys have been used successfully for turbine blades in high performance aircraft engines. The low cycle fatigue (LCF) lives of first generation SC superalloys were typically better than their polycrystalline counterparts by an order of magnitude. This improved fatigue behaviour has been attributed to a change in the mode of crack propagation from intergranular in the conventionally cast (CC) to transgranular in single crystals [3].

An important design criterion in gas turbine airfoil blades is the effect of thin-section size on creep resistance and creep rupture properties of the turbine blade alloys, since the blades used in the first row of the turbine in particular contain complex patterns of cooling holes with a thin wall (~ 1 mm) of uniform cross-section [4]. It is well known that the creep properties of the nickel-base superalloys can deteriorate markedly at thin-section sizes [4–10] ; a significant loss of properties has been reported for thinner sections. On investigation of the combined effects of thin-section size, carbide and cavity distributions using the CC MAR-M002 superalloy it was shown [8] experimentally that the creep rupture life was controlled by the $(d_c/a_0)/D$ ratio, where D is the diameter of the gauge section, d_c the cavity size and a_0 the carbide particle size; below a critical value ($\sim 100 \times 10^{-6}$ μm^{-1}) of this ratio the rupture life extends rapidly. An approximate linear correlation has been observed between the creep rupture strain (or ductility) and the $(d_c/a_0)/D$ ratio. In addition to the above-mentioned conclusions, it was also observed [9] that the creep rupture strain was controlled by the $[D^2/(n_G l)]$ ratio, where n_G is the number of grains per cross-section of specimen and l the half-cavity spacing.

2. Experimental procedure

In the present investigation the single crystal (SC) MAR-M 0 0 2 commercial superalloy has been used to investigate the effects of specimen thin-section size and cavitation on the creep properties of this alloy. The bulk composition of this alloy by wt % is: 0.5 C, 9.0 Cr, 5.5 Al, 10 W, 2.5 Ta, 1.5 Ti, 10 Co, 1.5 Hf and balance nickel. The single crystal creep specimens along the ⟨0 0 1⟩ crystallographic direction with a growth rate (or withdrawal rate) of 3 mm min^{-1} were used. The creep specimens were heat treated as follows before machining to suitable gauge section diameter of the creep specimens: 1225 °C for 2 h (solution treatment) plus 1030 °C for 12 h (coating cycle) plus 870 °C for 16 h (ageing cycle). The creep testing was carried out up to failure at 1173 K (900 °C) by uniaxial constant load testing in air, and the initial stress was 300 MPa. Heat treated and machined creep specimens with varying gauge diameter, D, from ~ 1.5 to 4.5 mm were used. The temperature variation over the testing time was kept constant within ± 0.5 K. The creep elongation was recorded continuously using differential transformers. The metallographic measurements on cavitation after creep fracture were

0022–2461

made using scanning electron microscopy (SEM) and the Cambridge Instrument, Q520 system.

3. Results

3.1. Microstructure

The microstructure of cast MAR-M002 is complex and consists of a high volume fraction of carbide and γ' phases in face centred cubic (FCC) solid solution γ matrix. The main microconstituents are illustrated in Fig. 1. The solid-rich last liquid at the end of solidification (1493 K) [11] forms degenerate and rosette type γ/γ' eutectics, which lie in interdendritic regions (Fig. 1a). The primary γ' phase, however, precipitates as ogdoads (Fig. 1b) on cooling below 1500 K with spheres of secondary γ' developing in the matrix at temperatures below about 1300 K [12]. In addition, the primary carbides, as shown in Fig. 1a, exist in several forms. MC type carbides with M = Ti, Ta, W or Hf appear near the liquidus of the alloy (roughly 1603 K) [11]. They are mainly located in the interdendritic area and appear as a Chinese character or distinct globular particles which form probably at about 1673 K [11]. Second type MC forms in the interdendritic areas, which are enriched mainly in Hf and depleted in W [11].

3.2. Creep

The effect of specimen gauge diameter, D, on the creep properties is shown in Fig. 2, which indicates that there are no correlations between the creep rupture life, t_R, creep rupture strain, ε_R, and the minimum creep rate, $\dot{\varepsilon}_m$, for the SC MAR-M002 alloy. The plotting of the creep rupture life against the cavity size, d_c, is given in Fig. 3a, which indicates a correlation between t_R and d_c, where $d_c = [f_c/(\pi N_A)^{1/2}]$, where f_c is the volume fraction of cavity and N_A the number of cavities per cross-section. However, the rather large scatter shown in this curve can be reduced to a much less value if t_R is replotted against the cavity size to specimen gauge section size, d_c/D, as seen in Fig. 3b. This rather good correlation (Fig. 3b) indicates that the creep rupture life improves rather rapidly with increasing d_c/D ratio; increasing this ratio from almost zero to approximately 200×10^{-5} t_R also increases from almost zero to approximately 500 h. The comparison of Figs 2, 3a and 3b indicates that the main factor affecting the creep rupture life is the cavity size; specimen section size has a less influential effect on t_R. Fig. 3 appears to indicate also that the cavity nucleation starts as soon as creep deformation initiates; reducing the cavity size to a very small value,

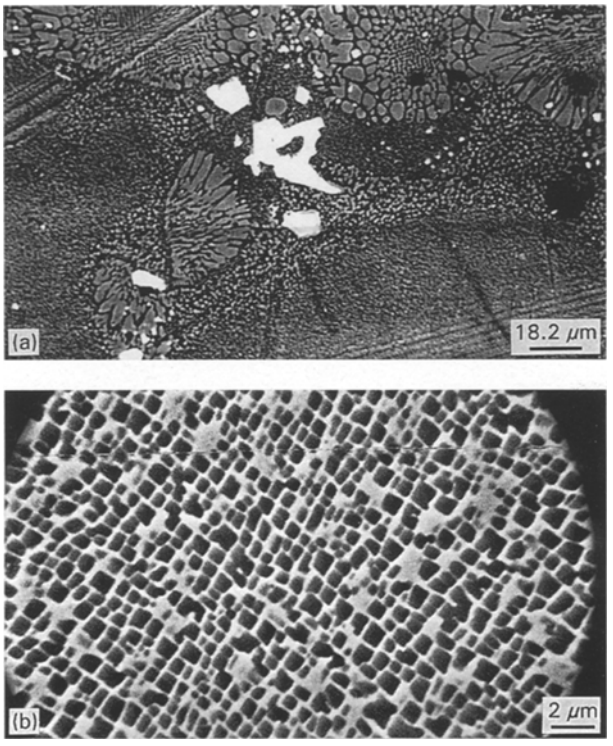

Figure 1 Initial distribution of microstructural features of the SC MAR-M002 produced along the ⟨001⟩ crystallographic direction with a withdrawal rate of 3 mm min^{-1} and heat treated: (a) rosette type $\gamma + \gamma'$ eutectic pools, as well as carbide morphology, and (b) cuboidal (or ogdoad) type primary γ' particles.

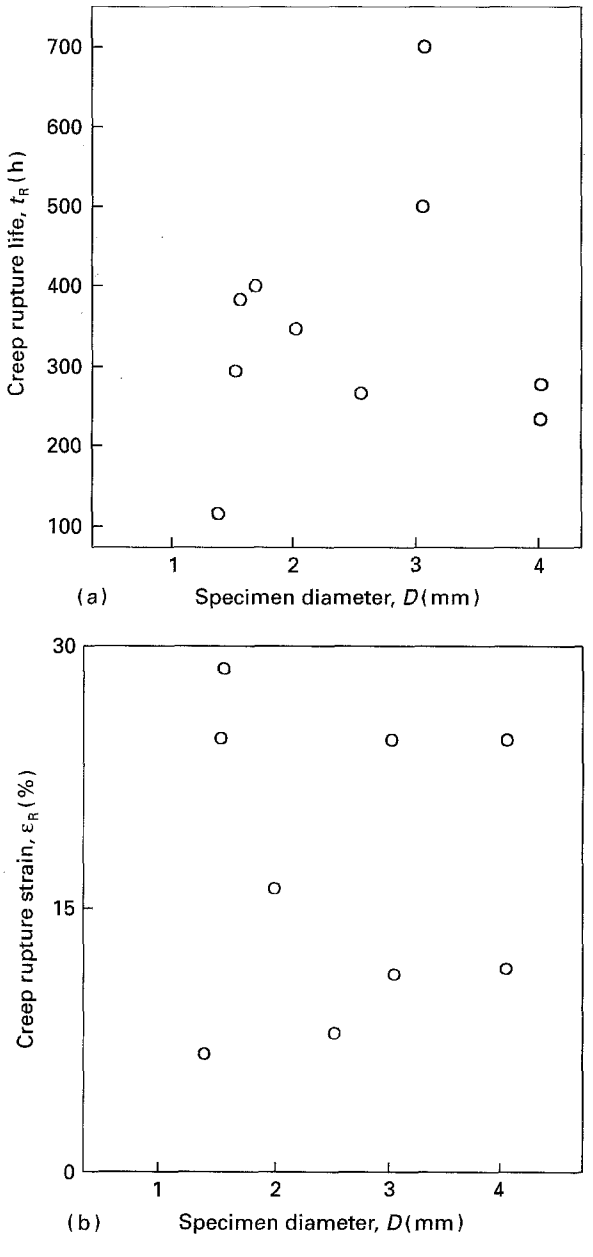

Figure 2 (Continued)

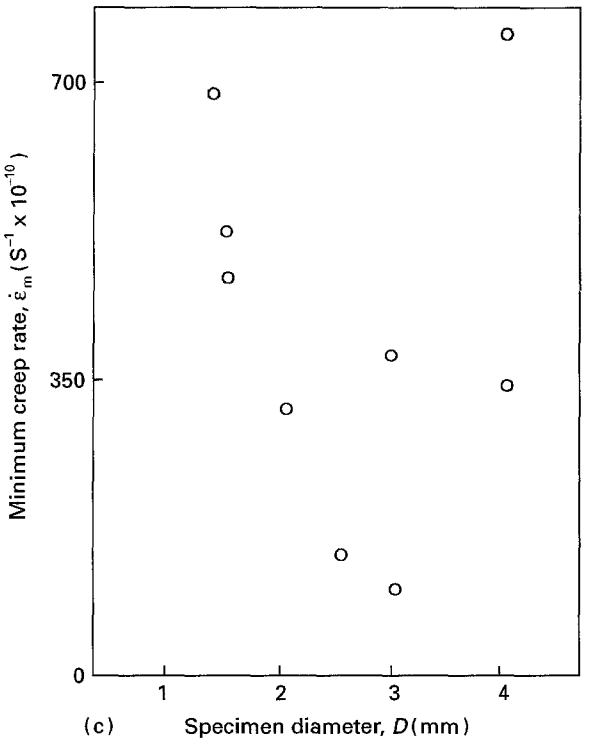

Figure 2 Effect of specimen gauge diameter, D, on creep properties: (a) t_R versus D, (b) ε_R versus D, and (c) $\dot{\varepsilon}_m$ versus D.

t_R approaches to zero value as well. The behaviour of t_R versus d_c/D ratio plot for the SC MAR-M002 (Fig. 3b) is opposite to that for the CC MAR-M002 (Fig. 4) [13]. As Fig. 4 illustrates, reducing the d_c/D ratio below a critical value ($\sim 5 \times 10^{-4}$) rapidly improves the creep ruputre life of the CC MAR-002 by a factor of four.

The effect of this ratio (d_c/D) on both the creep rupture strain and the minimum creep rate is given in Fig. 5. Although there is scatter (especially rather large scatter in Fig. 5a) in the data, these plots suggest that reducing this ratio seems to improve creep rupture ductility (Fig. 5a); whereas the creep resistance, i.e. $\dot{\varepsilon}_m$, deteriorates when reducing the ratio (Fig. 5b). The large scatter in the data indicates that the d_c/D ratio is not the main factor controlling ε_R. Fig. 6 shows the characteristic cavity morphologies observed from the fractured creep specimens. Fig. 6a illustrates a cavity morphology representing the point (A) in Fig. 3b. This micrograph shows that the cavity morphology is a helical (or zig-zag) type passing through the eutectic regions. The specimen representing this cavity morphology has the lowest creep rupture life observed (Fig. 3b). The micrograph in Fig. 6b corresponds to a cavity morphology at the point (B) in Fig. 3b. In this micrograph the morphology is still similar to that in Fig. 6a. Fig. 6c illustrates elongated or crystallographic type morphology, representing the point (C) in Fig. 3b, which starts to nucleate from a round shape carbide particle and stops to propagate in the eutectic region. Fig. 7 illustrates the effect of the mean cavity density, N_A, on the creep rupture life, which shows a sharp increase and decrease in t_R with increasing cavity density. The round shape cavity morphology representing the point (D) in Figs 3b and 7 is shown in Fig. 6d [the other points (A, B, C, D) in Fig. 7 correspond to those micrographs in Fig. 6a–d].

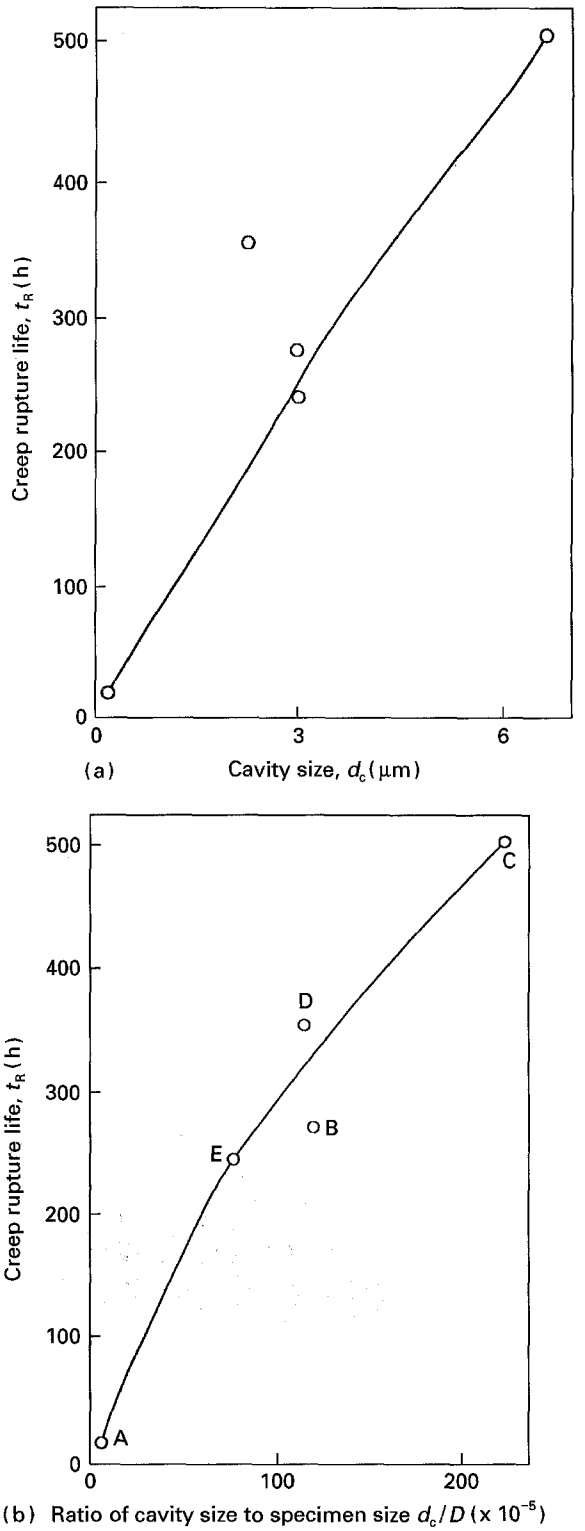

Figure 3 Combined effects of cavity (or microcrack) size, d_c, and thin-section size, D, on the creep rupture life: (a) effect of cavity size, d_c, on t_R (increasing d_c approximately linearly increases t_R with some scatter in the data), and (b) effect of the d_c/D ratio on t_R (indicating a similar relationship with that in Fig. 3a, but with much less scatter in the data).

4. Discussion

4.1. Combined effects of thin-section size and cavitation

An investigation of the fractured surfaces (Fig. 6c) has indicated that cavitation (or microcracking) on carbides or decohesion of the carbide–γ–matrix interface existed in the single crystal (SC) MAR-M002. In

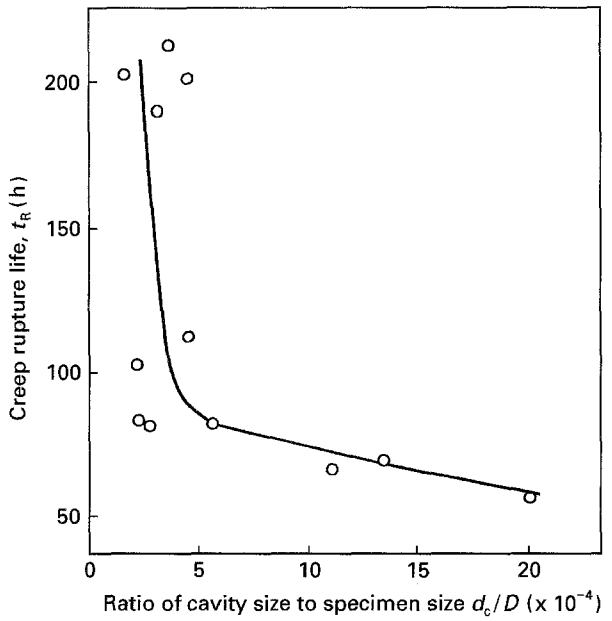

Figure 4 Effect of cavity size to specimen size ratio, d_c/D, on creep rupture life in conventionally cast (CC) MAR-M 002; reducing this ratio below a critical value ($\sim 5 \times 10^{-4}$) improves the creep rupture life by a factor of four [13].

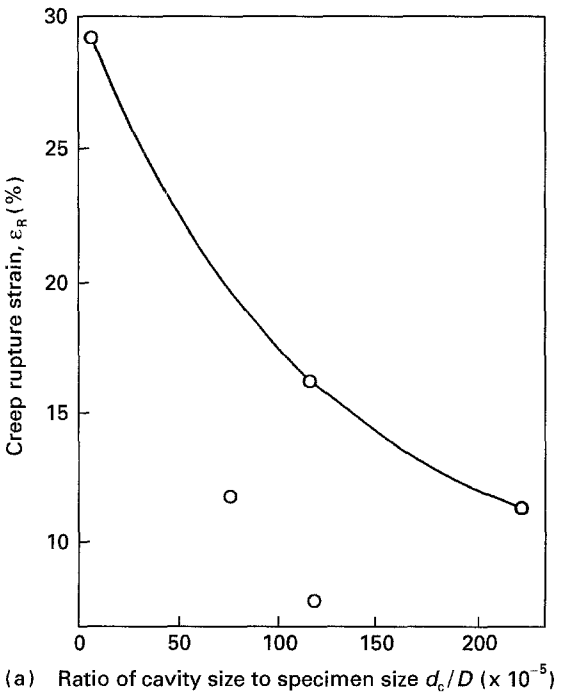

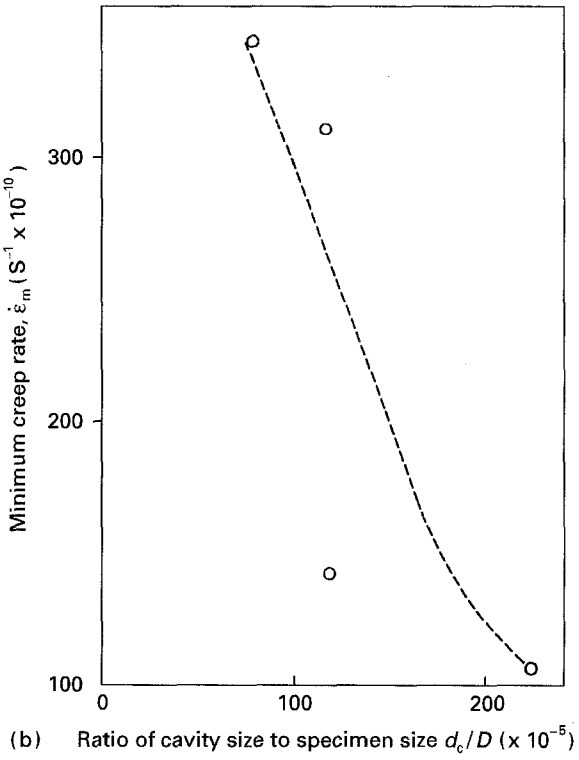

Figure 5 Effect of d_c/D ratio on creep rupture strain and minimum creep rate: (a) ε_R versus d_c/D ratio, and (b) $\dot{\varepsilon}_m$ versus d_c/D ratio.

addition to it, microcracking has also occurred either on the porosity sites, such as in Fig. 6d, or in the eutectic regions, Fig. 6a, b. Whereas in an investigation of the thin-section size effect for the CC MAR-M002, as reported previously by the present author [8, 9], microcracking has occurred as discrete and elongated types on carbides along the serrated grain boundaries, and massive type cavitation in the vicinity of the ($\gamma + \gamma'$) eutectic pools. It is therefore concluded that the major differences in behaviours of the creep rupture life as a function of the cavity size to specimen diameter, d_c/D, Figs 3b and 4 are due to the differences in the cavitation process taking place in the SC and CC MAR-M002 alloy. Several microstructural parameters, including the volume fraction, size and distribution of γ' precipitates [14, 15] and carbides [16, 17], dendritic structure [10], casting porosity [18], etc., can strongly affect the creep strength of the nickel-base superalloys. Specifically, the casting pores can strongly influence creep fracture behaviour in single crystal nickel-base alloys, although such effect has been studied rarely. In the absence of grain boundaries, carbide particles, eutectic regions, brittle phases or incipient melting (or low melting) regions, porosity sites represent the most effective sites available for the initiation of cracks. The sharp straight surfaces beteween the cracks (such as in Fig. 6a, c) indicate propagation of the cracks along the crystallographic directions. In MAR-M002 single crystals [19, 20], the fatigue deformation structure was shown to be inhomogeneous with planar octahedral slip. Crack initiation occurred at carbides or micropores. In the present result there is evidence that the crack initiated on carbides (or between carbide–γ–matrix interfaces) and propagated by the cleavage of γ–matrix and stopped in the solutionized ($\gamma + \gamma'$) eutectic regions (Fig. 6c). It was shown [21] that, at a temperature of 600 °C and a frequency of 10 Hz, fatigue cracks propagated in single crystals of MAR-M002 through the matrix, along {001} cube planes. On the basis of the present observation the cracks may be classified as follows

1. the round shape cavity morphology occurred on the porosity sites (Fig. 6d);
2. the zig-zag (or helical) type crack morphology (Fig. 6a, b); and
3. the elongated and sharp crack morphology (Fig. 6c).

From the present observations and past experimental results on SC MAR-M002 the cracks in

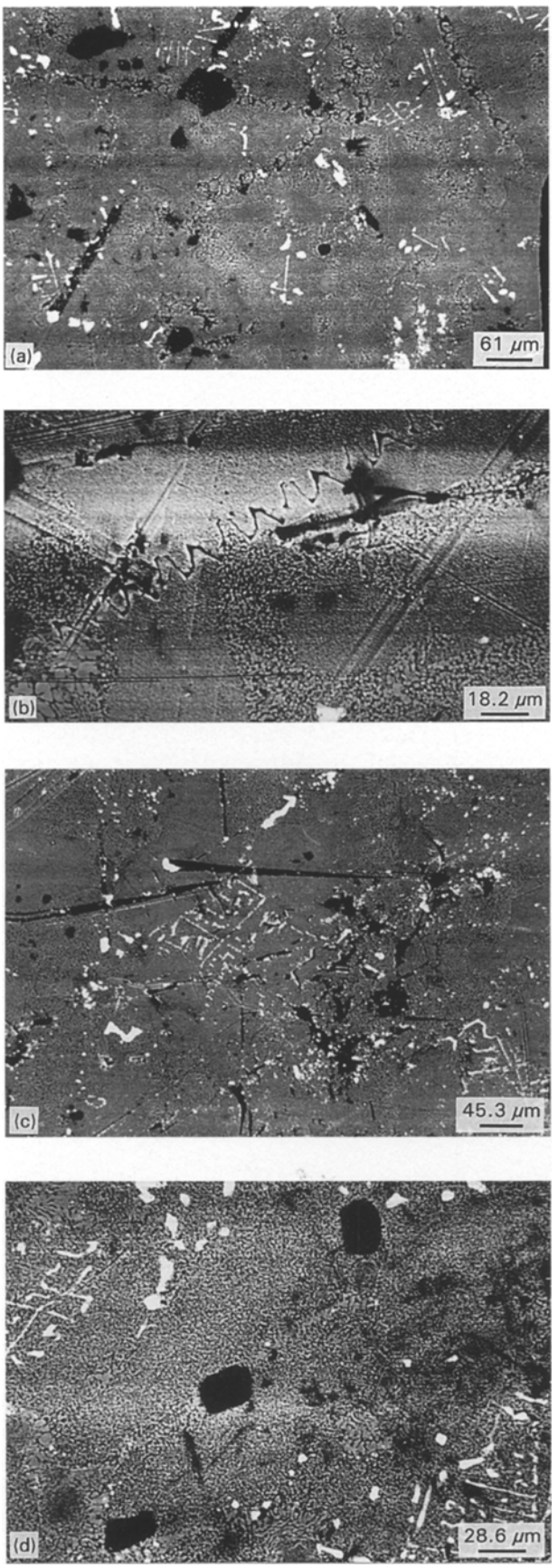

Figure 6 Typical microcrack (or cavity) morphologies observed after creep fracture: (a) helical shape cavity morphology corresponding to point (A) in Figs 3b and 7, passing through the eutectic regions; (b) zig-zag (or helical) shape microcrack morphology representing point (B) in Figs 3b and 7; (c) elongated and sharp microcrack morphology extending from a round shape carbide particle to the eutectic region [corresponding to the point (C) in Figs 3b and 7]; and (d) Round shape cavity morphology representing points (D) and (E) in Figs 3b and 7.

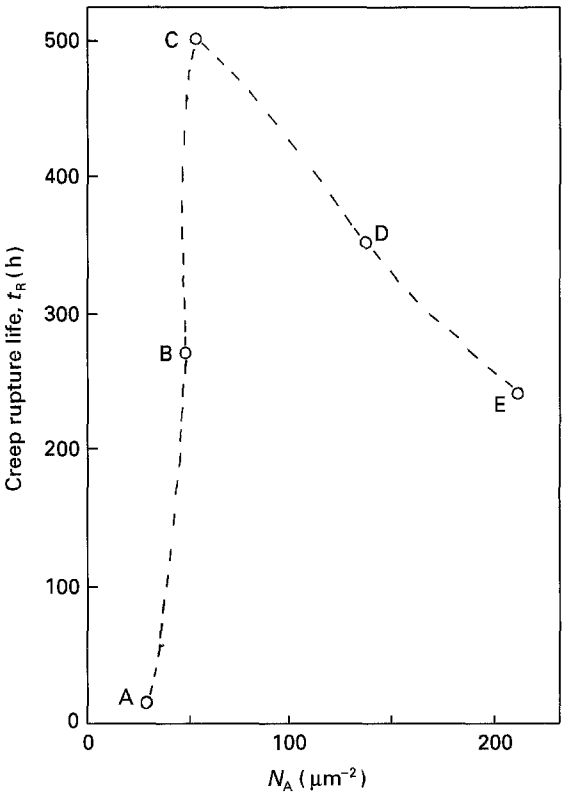

Figure 7 Effect of mean cavity (microcrack) density, N_A, on the creep rupture life, t_R.

points one and two may be schematically characterized as in Fig. 8. As Fig. 8a shows, zig-zag (or helical) crack propagation has occurred along the {0 0 1} planes (or ⟨0 0 1⟩ directions) of γ/γ' interfaces, since the primary γ' particles have usually cube-like morphology (see Fig. 1b) orientated along the {0 0 1} planes [22]. As the occurrence of the cuboid like (or ogdoad type) γ' particle morphology on the {0 0 1} planes ensures the relatively lower energy state between γ/γ' interfaces, it is possible that crack propagation, as in the case of Fig. 6b, has followed this lower energy path. The second type sharp and elongated crack morphology nucleates between the round shape carbide particle and γ–matrix interfaces (decohesion), and propagates along the ⟨0 0 1⟩ directions, and stops propagation in the solutionized $(\gamma + \gamma')$ eutectic pools (Fig. 8b). Lower crack propagation would be expected for these type of rather sharp cracks (such as in Fig. 8b) in samples with large amounts of $(\gamma + \gamma')$ eutectic pools, as these regions are relatively ductile areas within the microstructure. That is, as the eutectic regions are softer than the dendrite cores, the eutectic regions could deform plastically and inhibit the crack growth necessary for final fracture.

The creep rupture lives of SC MAR-M 0 0 2 (Fig. 3b) were significantly longer than those for equiaxed (or CC) MAR-M 0 0 2 (Fig. 4) as a variation of d_c/D ratio. The higher creep rupture lives for SC MAR-M 0 0 2 may be attributed to the following reasons

1. the absence of grain boundaries which are usually the weak locations against creep deformation; and
2. correct heat treatments applied lead to an optimum γ'–precipitate morphology in terms of size, shape, and volume fraction, which yield the optimum

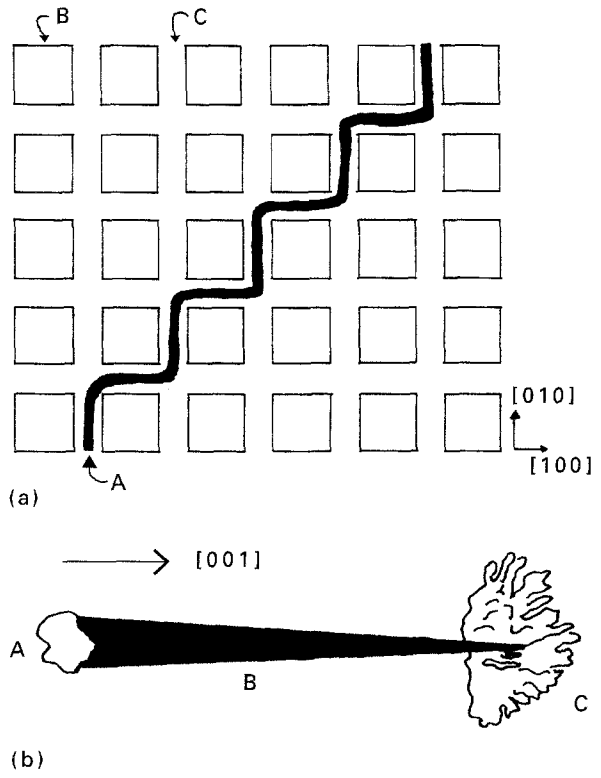

Figure 8 Schematic representation of microcracks (cavities) observed in SC MAR-M002: (a) the zig-zag (or helical) type microcrack morphology (microcrack propagation occurs along the ⟨001⟩ crystallographic directions between the γ/γ' interfaces). (A) crack propagation path, (B) cuboidal type γ' morphology, (C) γ–matrix between γ'–particles; and (b) elongated and sharp microcrack morphology [the crack nucleates between the round shape carbide particle and γ–matrix interface (decohesion), propagating along the ⟨001⟩ directions, and stops in the solutionized $(\gamma + \gamma')$ eutectic pools] (A) carbide particle, (B) microcrack, (C) $(\gamma + \gamma')$ eutectic pool.

creep properties; homogeneously distributed cube-shaped fine γ' precipitates provide high creep resistance to deformation [23].

Assuming that $D/d_c = N_m$ indicates the total number of the mean-sized cavity (crack) particles across the gauge section of the specimen, Fig. 3b therefore indicates that reducing the total number of cavities in the gauge cross-section, N_m, continuously improves the creep rupture life. Extrapolating N_m to a very high value would yield to almost zero creep rupture life. This indicates that the creep life of the SC MAR-M002 can be improved considerably by reducing the available potential cavity nucleation sites, such as carbide particles, porosity sites and γ/γ' eutectic regions. While carbon additions are beneficial for grain boundary ductility, the large carbide can adversely affect creep ductility [16]. When polycrystalline alloys were cast in SC form it was determined that carbides did not impart any beneficial strengthening effects [23] in the absence of grain boundaries, such as in the present alloy, and thus could be eliminated. In fact, in the new generation SC alloys all the grain boundary strengtheners, i.e. B, Zr, Hf, including carbon were eliminated. Microporosity, which is present in various amounts in all castings, resulting from the shrinkage liquid metal, is the prime site for microcrack nucleation in carbon-free alloys [23].

In conclusion, the occurrence of microcrack nucleation rapidly deteriorates the creep strength contributed mainly by the γ' particle deformation in the γ–matrix, as is evident in Fig. 3b. Hence, deterioration of the creep rupture life can be prevented by reducing the nucleation of microcracks or, equivalently, by increasing the mean spacing between microcracks, but it is difficult [24] to change these parameters by more than a factor of five or so. Whereas in the case of the CC MAR-M002 (see Fig. 4), improvement in creep rupture life is associated with reducing the stress concentrations by inhibiting cavity nucleation on carbide particles along the grain boundaries [8, 9].

The loose effect of $N_m = D/d_c$ on creep resistance, $\dot{\varepsilon}_m$ has also been observed. Namely, the creep resistance of the alloy may be improved by reducing the total number of mean sized microcrack particles (Fig. 5b). Improvement in the creep rupture life and creep resistance by reducing N_m may lead to a reduction in creep ductility (Fig. 5a), although the rather large scatter in the data indicates N_m does not control fully the ductility. The creep rupture ductility has been replotted against a new parameter, D^2N_A, as illustrated in Fig. 9. $(D^2N_A) \propto [(\pi D^2 N_A)/4]$ is the actual total number of microcrack particles, N_T, observed in the gauge cross-section, D; where N_A is the mean number of microcrack particles per gauge cross-section (microcrack particle density). As Fig. 9 indicates, there is a rather good correlation between ε_R and $N_T (\propto D^2 N_A)$. A rapid improvement in creep ductility can be made by increasing the total number of microcrack particles, N_T; increasing N_T twice, ε_R can be improved by a factor of about three, i.e. from ~5 to ~30% strain. One is of the opinion that the variability of cavity rates follows naturally from the variability in potential cavitation nucleation sites, such as microporosity and carbide particles, as well as the solutionized eutectic pools available in the microstructure.

The models developed by Dyson and coworkers [7, 25] suggest that the lifetime of environmentally damaged solid specimens is proportional to the square of their radius (assumed that the damage propagates inward from the surface), apart from other factors affecting the creep life. An investigation [26] of the thin-section size effect on directionally solidified (DS) MAR-M002 has shown that this alloy did not have a large reduction in the creep rupture life of thin-section castings between 760 and 930 °C. However, the same study at 1040 °C did show a reduction in creep rupture life in the thin-sections. This loss of creep life was believed [26] to result from oxidation effects. Therefore, it is concluded that at the present test temperature (900 °C) oxidation would not be expected to be the important mechanism for SC MAR-M002.

Brittle fracture, caused by a critical number of inhomogeneities, gives rise to the statistical aspect of fracture [27]; that of increasing probability of fracture with increasing volume (or area or length). Therefore, an explanation for the thin-section size effect can be provided also by statistical distribution of microcracks in the microstructure. It is generally believed that brittle fracture is controlled by a distribution of microcracks, which the fracture stress, σ_F, might be

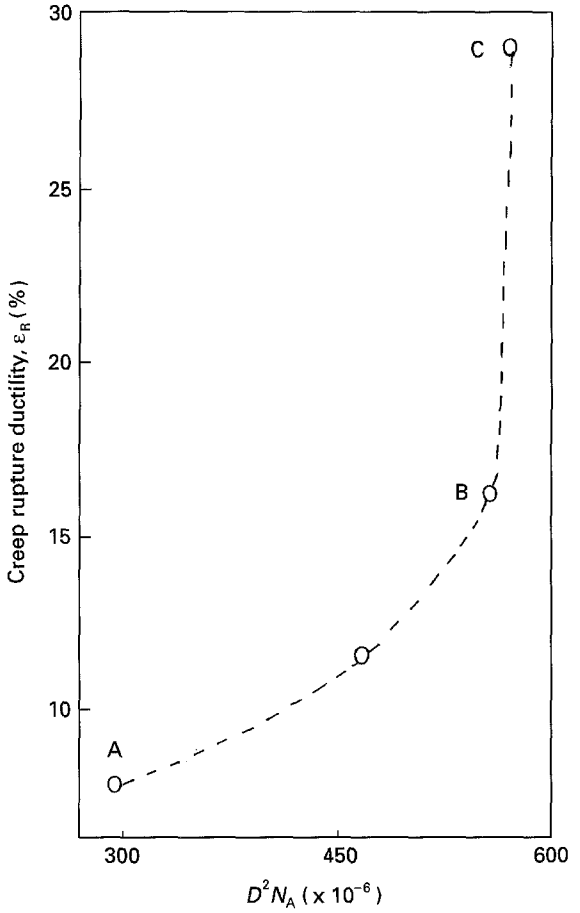

Figure 9 Rapid improvement in the creep rupture ductility, ε_R, by increasing the total number, N_T, of microcrack particles across the gauge cross-section, $D^2N_A \propto N_T$.

approximated by the Griffith equation

$$\sigma_F = A\ [(2E\ \gamma_F)/(\pi\ d_i)]^{1/2} \qquad (1)$$

where E is Young's modulus of elasticity, γ_F the fracture surface energy (J m^{-2}), A a geometrical constant and d_i the microcrack size of the ith particle in the statistical distribution of total microcrack particles, N_T. For every size of microcrack, d_i, there will be a certain fracture stress, σ_F, determined by Equation 1. Here it is assumed that the specimen is made up of many small volume elements, which each contain a single microcrack and no interaction between the microcracks in the different volume elements. In this assumption [28] the strength of the specimen is determined by the element which contains the longest microcrack size (Equation 1). Therefore, the fracture strength is determined, not by an average (or mean) value of the size distribution of microcracks (or cavities), but by the longest (or most dangerous) microcrack. This concept of brittle fracture is known as the weakest link, or "largest flaw", concept.

According to this concept, as the volume of the specimen (or section size) increases the total number of microcracks also increases, as can be suspected in Fig. 9, and therefore the probability of encountering a severe microcrack is normally increased. However, one should look at the observed distribution function of the small value of fracture strength against the number of microcracks for a given distribution function of microcrack sizes. If it is assumed that the distribution of microcrack size is to be Gaussian, which indicates the probability of having a small crack is the same as the probability of occurrence of large crack [27], then for a Gaussian distribution of the strength of the weakest element, the strength should decrease linearly with increasing $(\log V)^{1/2}$, where V is the volume of the specimen, which does not agree with the present observation (Fig. 9). In the past Weibull's distribution function (extreme value distribution) has also been used to describe the microcrack size distribution [27–29]. If the effect being observed is due to the smallest or largest of a number of variables, a Weibull distribution is to be expected. For this frequency distribution, the cumulative distribution function is given

$$P(d_i) = 1 - \exp\ \{ - [(d_i - d_u)/d_0]^m\} \qquad (2)$$

where $P(d_i)$ is the probability that a value less than microcrack length d_i will be obtained, d_u is the value of d_i for which $P(d_i) = 0$, and d_0 and m are constants. Observed microcrack size (as area) histograms (distributions) in Fig. 10a, b and c corresponds to the points (A)–(C) in Fig. 9, respectively. Comparison of these three histograms indicates that the significant higher proportions of microcrack particles become much smaller in size when going from point (A)–(C) in Fig. 9. This observation confirms the Weibull distribution function in the weakest link concept, that the higher the total number of microcracks by increasing the specimen section size ($N_T \propto D^2N_A$) increases the probability to have less dangerous microcracks (smaller size distribution).

An investigation by the present author [9] on the CC MAR-M002 has shown that the creep rupture strain is controlled by the $[D^2/n_G \cdot l)]$ ratio. When n_G approaches unity, i.e. $n_G \rightarrow 1$, which is the single crystal condition, it is expected that the creep rupture strain must be controlled by the (D^2/l) ratio, i.e. what the present observation on the SC MAR-M002 indicates.

To summarize, as the present observation shows, the rapid improvement in creep rupture ductility with a total number of microcracks across the gauge cross-section ($N_T \propto D^2N_A$) is due to the increase in proportion of the less dangerous microcracks. Furthermore, while creep rupture ductility is sensitive to the crack size distribution, the creep rupture life depends very much on the number of mean-sized microcracks ($N_m = D/d_c$) across the gauge diameter. As Argon [30] pointed out, microcrack nucleation is a key step in creep fracture, the suppression or postponement of crack nucleation can improve creep life considerably for SC MAR-M002.

An important question is whether tertiary creep results from cavitation and microcrack growth as in the present observation, rather than from a directly diffusion dependent process. Fig. 11 shows the effect of the cavity volume fraction to specimen diameter ratio, f_c/D, on the creep rupture ductility, ε_R. A possible explanation of Fig. 11 can be given by the theoretical treatment of Thomason [31]. The model of Thomason is able to treat the effects of cavity volume fraction on

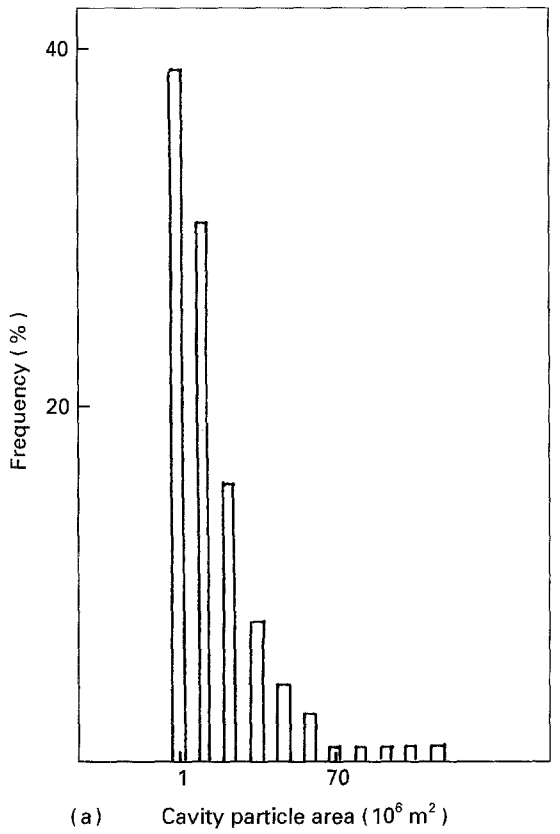

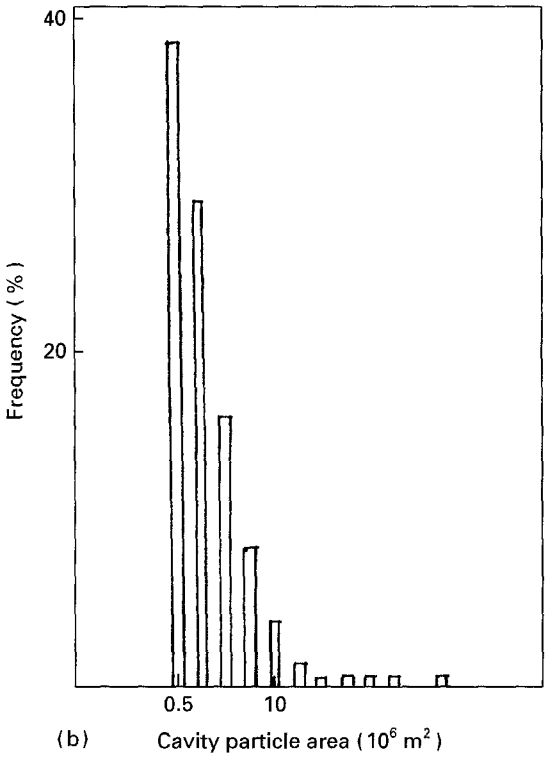

Figure 10 Three microcrack size (as area) histograms (distributions), corresponding to: (a) point A, (b) point B, and (c) point C in Fig. 9.

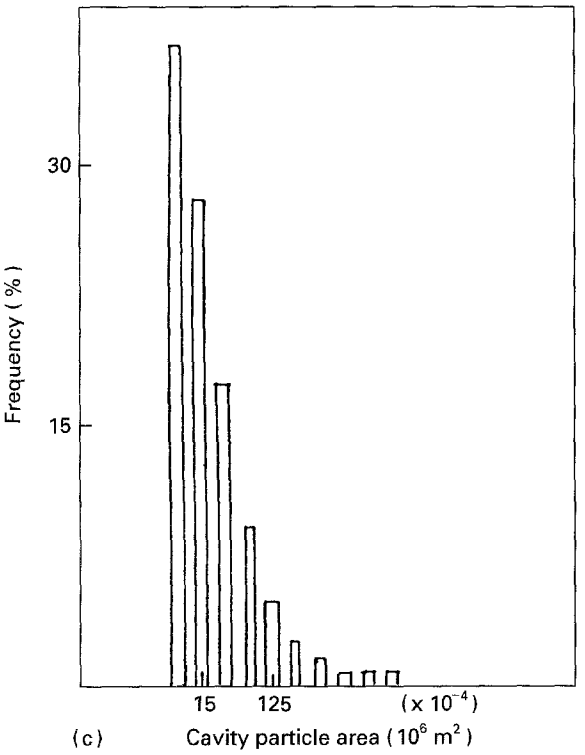

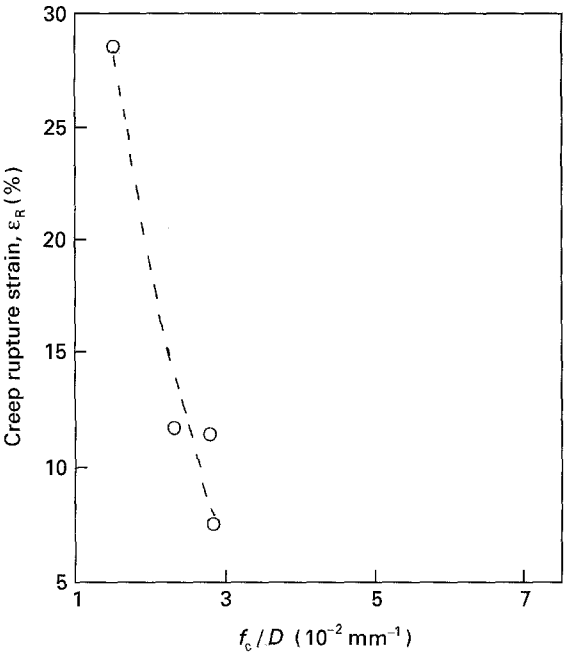

Figure 11 Effect of the cavity volume fraction to specimen gauge diameter ratio, f_c/D, on the creep rupture strain, ε_R.

ductility in a uniaxial tension stress field ahead of a sharp microcrack

$$\varepsilon_R = (1/2) \ln\{d_c/[L f_c^{1/2}(1 - f_c^{1/2})]\} \quad (3)$$

where $L = 2l = 0.5/(N_A)^{1/2}$, is the cavity spacing. The curve in Fig. 11 is similar in shape to that for the theoretical ε_R versus f_C [31], which suggests that the present result is broadly in agreement with Thomason's model, though the section size effect is not included in this model. According to Thomason's model, ε_R might be described as the mechanical post-instability strain to fracture. If one considers creep deformation under full structural stability (as postulated in Thomason's theory), one can assume the creep rate, $\dot{\varepsilon}$, –stress, σ, relation (power law creep) to be obeyed for all creep deformation. It follows that the power law creep ($\dot{\varepsilon} = B\sigma^n$) can be integrated from deformation to rupture (where n is the stress sensitivity

exponent and B is the constant). That is what Fig. 12 shows broadly, though there is some scatter in data

$$\varepsilon_R \propto \dot{\varepsilon}_m t_R \ (= C_M) \quad (4)$$

$$\varepsilon_R = B \sigma^n t_R \quad (5)$$

Equation 4 or 5 shows a clear similarity to Thomason's relationship, indicating that creep rupture strain or ductility is mainly determined by conditions for mechanical instability.

4.2. Creep life prediction

For the design of components, knowledge of the creep rupture behaviour is of great interest. In designing a plant, a prerequisite is knowledge of the service conditions which the component will be operating and how the material will behave under such conditions. Many empirical relationships have been proposed [32–35] to analyse data from accelerated uniaxial constant load creep tests. A relation between fracture time and minimum creep rate has been observed by a number of authors. According to Monkman and Grant [32], a certain relation between creep rupture life, t_R, and the minimum creep rate, $\dot{\varepsilon}_m$, holds for many creeping relatively simple alloys, which is given by

$$\dot{\varepsilon}_m^{\beta} t_R = \text{constant} \quad (6)$$

since β is near unity, the Monkman–Grant relation is often cited as

$$\dot{\varepsilon}_m t_R = C_M \quad (7)$$

The "constant", C_M in Equation 7 is sometimes called the Monkman–Grant "ductility", which is of the nature of a strain. The Monkman–Grant relationship (Equation 7) is the most powerful, as well as the simplest, method of predicting creep life available, which offers the possibility of long term extrapolation if the same creep deformation mechanism operates during the whole creep life [17]. An explanation for this relationship is to assume that not only is the fracture process, i.e. both nucleation and growth of cavities, controlled by deformation, but that it occurs by a mechanism of deformation rather than, for example, diffusion. In the present investigation there is no relation between $\dot{\varepsilon}_m$ and t_R, as well as specimen section size, D, for SC MAR-M002. An investigation of CC MAR-M002 by the present author [36] reveals that a relation between $\dot{\varepsilon}_m$ and t_R does not exist, but there is quite good linear correlation between t_R/d_G and $\dot{\varepsilon}_m/D$ ratios on log–log scales, where d_G is the grain size. Fig. 13 illustrates the dependence of the Monkman–Grant ductility on the $[f_c/(1-f_c)]$ ratio; ductility, which refers to the extent to which a material can deform plastically before fracture, continuously increases with this ratio. Here the ratio $f = [f_c/(1-f_c)]$ is proportional to the amount of microcrack volume to the effective specimen volume ratio, i.e. $[\pi D^2 f_c/4]/[(\pi D^2)\ (1-f_c)\ /4]$, which further confirms that ductility is determined by conditions for mechanical instability. Therefore, increasing the relative cavity volume fraction with respect to the effective specimen volume improves the Monkman–Grant ductility.

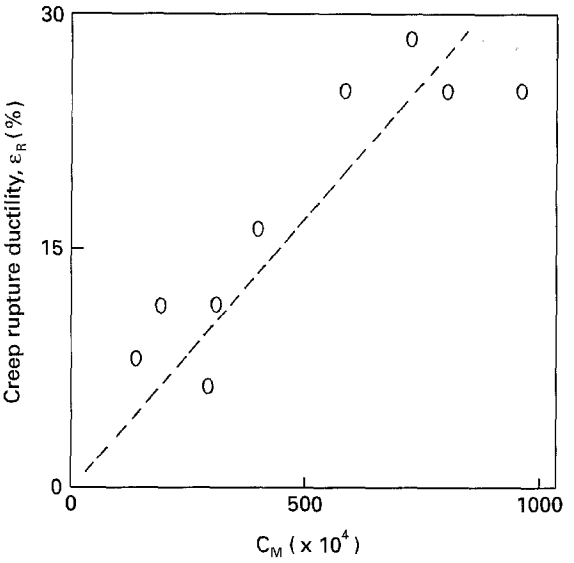

Figure 12 Correlation between the creep rupture ductility, ε_R, and the product of the minimum creep rate and creep rupture life, i.e. $C_M = \dot{\varepsilon}_m t_R$.

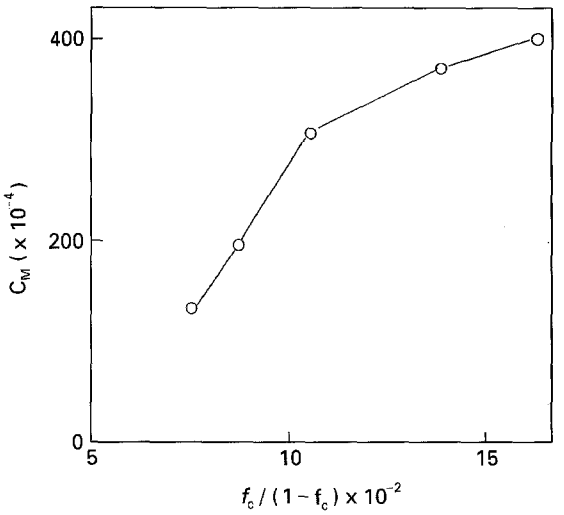

Figure 13 Dependence of the Monkman–Grant ductility, C_M, on the $[f_c/(1-f_c)]$ ratio.

Dobes and Milicka [33] proposed another relation by the inclusion of a normalizing parameter of rupture strain, ε_R, to modify Equation 7, i.e.

$$(t_R \dot{\varepsilon}_m)/\varepsilon_R = C^* \quad (8)$$

where C* is a constant. This relationship is given in Fig. 12 for the present alloy, which indicates a rather good correlation. This figure also indicates that the Dobes–Milicka relationship for SC MAR-M002 is independent of specimen section size, D, as was the case for the CC one as well [36].

Koul and coworkers [34] proposed the following new relationship based on the sum of the primary creep life, t_p, plus the secondary creep life, t_s, normalized by the sum of the primary creep strain, ε_p, plus the secondary creep strain, ε_s, varying as a function of minimum creep rate

$$(t_p + t_s)/(\varepsilon_p + \varepsilon_s)\ (\dot{\varepsilon}_m)^M = K \quad (9)$$

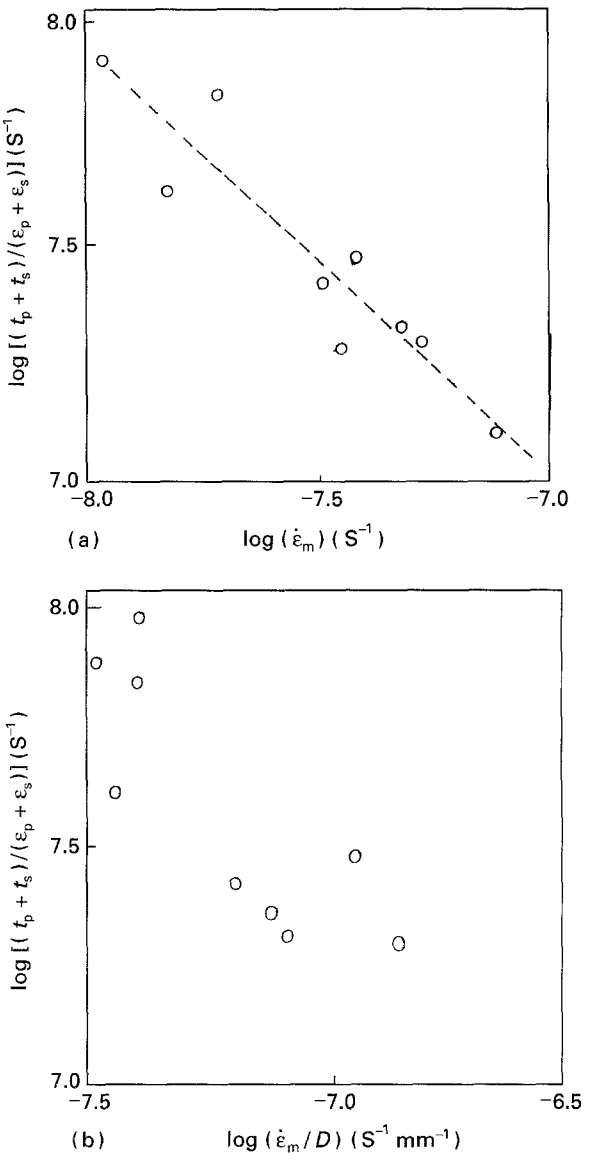

Figure 14 Relationship between various creep parameters and the specimen section size, D: (a) $[(t_p + t_s)/(\varepsilon_p + \varepsilon_s)]$ versus $\dot{\varepsilon}_m$ showing good linear correlation, Equation 9; and (b) $[(t_p + t_s)/(\varepsilon_p + \varepsilon_s)]$ versus $(\dot{\varepsilon}_m/D)$.

where M and K are constants. It was claimed that this relationship is independent of any changes in the predominant deformation mechanism. The plotting of Equation 9 on log–log scales is shown in Fig. 14a for the present SC MAR-M002, which shows a rather good linear correlation with small scatter in the data. Since the size of the specimen is varied, the $(t_p + t_s)/(\varepsilon_p + \varepsilon_s)$ ratio is also plotted against $\dot{\varepsilon}_m$ normalized by D, i.e. $\dot{\varepsilon}_m/D$, as shown in Fig. 14b, which indicates that Equation 9 is also independent of section size. It was suggested [34] that Equation 9 can be used to analyse service-induced degeneration effects by predicting the remaining useful life of turbine engine components. As Fig. 14a shows Equation 9 is also applicable to the present alloy (SC MAR-M002) despite the fact that the section size was varied.

5. Conclusions

The combined effects of thin-section size and cavitation on the creep rupture behaviour of SC MAR-M002 were studied at the creep conditions of 300 MPa and 900 °C and the following conclusions can be made

1. On the basis of the cavity nucleation sites the microcracks were classified as

(a) round shaped microcracks nucleating on microporosities;

(b) zig-zag (or helical) type crack morphology that propagate along the ⟨001⟩ crystallographic directions between the γ/γ' interfaces;

(c) elongated and sharp microcrack morphology (this crack nucleates between the carbide particle and γ-matrix interface, propagating along ⟨001⟩ directions, and stops in the $(\gamma + \gamma')$ eutectic regions).

2. The creep rupture life of the material is controlled by the crack size to thin-section size ratio, d_c/D, (or the total number, N_m), of mean-sized crack particles across the diameter, assuming $D/d_c = N_m$; reducing N_m continuously and rapidly extends the creep rupture life; reduction in N_m by a factor of about two improves t_R by a factor of about five.

3. The creep rupture ductility, ε_R, can be improved rapidly by increasing the total number of microcrack particles across the gauge cross-section of the specimen, $(N_T \propto D^2 N_A)$; increasing N_T by $\sim 100\%$ ε_R can be increased by as much as a factor of about five. ε_R variation against $(D^2 N_A)$ parameter was interpreted in terms of the weakest link concept; observation of the higher proportion of the less likely dangerous (smaller in size) microcracks with increasing $(D^2 N_A)$ parameter was the reason for the improvement in the creep rupture ductility.

4. The creep rupture ductility can also be interpreted in terms of the mechanical instability concept according to Thomason's model. Relative increase of internal damage with respect to the effective section size, i.e. $f_c/(1 - f_c)$ improves the ductility continuously.

5. Dobes–Milicka (Equation 8) and Koul *et al.* (Equation 9) relations developed for the prediction of creep life are independent of thin-section size effect for SC MAR-M002.

References

1. J. J. JACKSON, M. J. DONACHIE, M. J. HENRICKS and M. GELL, *Metall. Trans.* **8A** (1977) 1615.
2. M. GELL, D. N. HULL and A. F. GIAMEI, in "Proceedings of the Fourth International Symposium on Superalloys (Superalloys 1980) ", edited by J. K. Tien, S. T. Wlodek, H. Marrow, M. Gell and G. E. Maurer (American Society for Metals, Metals Park, OH, 1980) p. 205.
3. G. R. LEVERENT and M. GELL, *Trans. AIME* **245** (1969) 1167.
4. T. B. GIBBONS, *Metals Technol.* **8** (1981) 472.
5. E. G. RICHARDS, *J. Inst. Metals* **96** (1968) 365.
6. M. C. PANDEY, D. M. R. TAPLIN and P. R. RAO, *Mater. Sci. Engng* **A118** (1989) 33.
7. B. F. DYSON and S. OSGERBY, *Mater. Sci. Technol.* **3** (1987) 545.
8. A. BALDAN, *Z. Metallkd.* **85** (1994) 40.
9. *Idem, Mater. Trans., JIM*, submitted.
10. *Idem, J. Mater. Sci. Lett.* **13** (1994) 734.
11. P. VITAOUR, D. COUTSOURADIS and L. HABRAKEN, in "Proceedings High Temperature Alloys for Gas Turbines and Other Applications", Liege, 25–27 September, edited by D. Coutsouradis, P. Felix, H. Fischmeister, L. Habraken, Y. Lindblom and M. O. Speidel (Applied Science, London, 1978) pp. 875–891.

12. H. BURT, J. P. DENNISON, I. C. ELLIOT and B. WILSHIRE, *Mater. Sci. Engng* **53** (1982) 245.
13. A. BALDAN, Internal Report (CSIR, Pretoria, South Africa, 1992).
14. *Idem, Z. Metallkd.* **83** (1992) 324.
15. *Idem, ibid.* **83** (1992) 331.
16. *Idem, ibid.* **83** (1992) 750.
17. *Idem, J. Mater. Sci. Lett.* **11** (1992) 1315.
18. *Idem, ibid.* **26** (1991) 3879.
19. G. R. LEVERENT and M. GELL, *Metall. Trans.* **6A** (1975) 367.
20. M. GELL and G. R. LEVERENT, *Acta Metall.* **16** (1968) 553.
21. J. S. CROMPTON and J. W. MARTIN, *Metall. Trans.* **15A** (1984) 1771.
22. M. DOI, T. MIYAZAKI and T. WAKATSUKI, *Mater. Sci. Engng* **74** (1985) 139.
23. T. KHAN, "Proceedings, High Temperature Alloys for Gas Turbines and Other Applications", edited by W. Betz, R. Brunetaud, D. Coutsouradis, H. Fischmeister, T. B. Gibbons, I. Kvernes, Y. Lindblom, J. B. Marriot and D. B. Meadowcroft, Liege, Belgium, 6–9 October (1986) pp. 21–50.
24. W. D. NIX, *Mater. Sci. Engng* **A103** (1988) 103.
25. M. F. ASHBY and B. F. DYSON, in "Advances in Fracture Research (Fracture 84) ", Proceedings of the Sixth International Conference on Fracture (ICF6), New Delhi, India, Vol. 1, edited by S. R. Valluri, D. M. R. Taplin, P. Rama Rao, J. F. Knott and R. Dubey (Pergamon Press, Oxford, 1984) pp. 3–30.
26. M. R. WINSTON and J. E. NORTHWOOD, "Solidification technology in the foundary and cast house" (Metals Society, London, 1983) pp. 298–303.
27. C. LIPSON and N. J. SHETH, "Statistical design and analysis of engineering experiments" (McGraw-Hill, New York, 1973) pp. 36–44.
28. K. P. GEORGE, "Advances in Fracture Research (Fracture 84) ", Proceedings of the Sixth International Conference on Fracture (ICF6), New Delhi, India, Vol. 5, edited by S. R. Valluri, D. M. R. Taplin, P. Rama Rao, J. F. Knott and R. Dubey (Pergamon Press, Oxford, 1984) pp. 3549–3556.
29. W. WEIBULL, *Mater. Res. Studies* May (1962) 405.
30. A. S. ARGON, *Scripta Metall.* **17** (1983) 5.
31. P. F. THOMASON, "Ductile fracture of metals" (Pergamon Press, Oxford, 1990) pp. 19–20, 115–130.
32. F. C. MONKMAN and N. J. GRANT, *Proc. ASTM* **56** (1956) 593.
33. F. DOBES and K. MILICKA, *Met. Sci.* **10** (1976) 382.
34. A. K. KOUL, R. CASTILLO and K. WILLETT, *Mater. Sci. Engng* **66** (1984) 213.
35. R. W. EVANS, J. D. PARKER and B. WILSHIRE, "Recent advances in creep and fracture of engineering materials and structures", edited by B. Wilshire and D. R. Owen (Pineridge Press, Swansea, 1982) p. 135.
36. A. BALDAN, *J. Mater. Sci. Lett.*, submitted.

Received 4 August 1994
and accepted 22 March 1995